

# Effects of electron-phonon coupling in the Kondo regime of a two-orbital molecule

G. I. Luiz,<sup>1</sup> E. Vernek,<sup>1</sup> L. Deng,<sup>2</sup> K. Ingersent,<sup>2</sup> and E. V. Anda<sup>3</sup>

<sup>1</sup>*Instituto de Física, Universidade Federal de Uberlândia, Uberlândia, MG 38400-902, Brazil*

<sup>2</sup>*Department of Physics, University of Florida, P.O. Box 118440, Gainesville, Florida 32611-8440, USA*

<sup>3</sup>*Departamento de Física, Pontifícia Universidade Católica do Rio de Janeiro, RJ 22453-900, Brazil*

(Dated: August 3, 2012)

We study the interplay between strong electron-electron and electron-phonon interactions within a two-orbital molecule coupled to metallic leads, taking into account Holstein-like coupling of phonons to the molecular occupancies as well as phonon-mediated interorbital tunneling. By combining canonical transformations with numerical renormalization-group calculations to address the interactions nonperturbatively and on equal footing, we obtain a comprehensive description of the system's many-body physics. The electron-phonon interactions strongly modify the bare orbital energies and the Coulomb repulsion between electrons in the molecule, and tend to inhibit tunneling of electrons between the molecule and the leads. The consequences of these effects are considerably more pronounced when both molecular orbitals lie near the Fermi energy of the leads than when only one orbital is active. In situations where a local moment forms on the molecule, there is a crossover with increasing electron-phonon coupling from a regime of collective Kondo screening of the moment to a limit of local phonon quenching. At low temperatures, this crossover is associated with a rapid increase in the electronic occupancy of the molecule as well as a marked drop in the linear electrical conductance.

PACS numbers: 71.38.-k, 72.15.Qm, 72.10.Fk, 73.23.-b, 73.23.Hk, 73.63.-b, 73.63.Kv, 73.63.Rt

## I. INTRODUCTION

Single-molecule junctions<sup>1-4</sup> are structures consisting of a single molecule bridging the gap between source and drain electrodes, allowing electronic transport when a bias voltage is applied across the structure. These systems, which manifest a rich variety of experimentally accessible physics in a relatively simple setting,<sup>5</sup> have attracted much theoretical and experimental effort in connection with molecular electronics.<sup>6,7</sup> A major goal of these efforts has been to take advantage of natural or artificial molecules for technological purposes. Examples of single-molecule junctions encompass, for example, single hydrogen molecules<sup>8-10</sup> and more complex structures such as 4,4'-bipyridine molecules coupled to metallic nanocontacts.<sup>11-13</sup>

An important ingredient in transport through molecular systems is the electron-electron interaction (Coulomb repulsion), the effect of which is greatly enhanced by the spatial confinement of electrons in molecules.<sup>14</sup> Electron-electron (e-e) interactions are known to produce Coulomb blockade phenomena<sup>15</sup> and Kondo correlations at low temperatures.<sup>16,17</sup> Confined electrons are also known to couple to quantized vibrations (phonons) of the molecules,<sup>18</sup> resulting in important effects on electronic transport.<sup>19-27</sup> Single-molecule junctions therefore provide a valuable opportunity for studying charge transfer in systems with strong competing interactions.

It has recently been demonstrated that the energies of the molecular orbitals in a single-molecule junction can be tuned relative to the Fermi energy of the electrodes by varying the voltage applied to a capacitively coupled gate.<sup>28</sup> Similar control has for some time been available in another class of nanoelectronic device: a quantum dot coupled to a two-dimensional electron gas.<sup>29,30</sup> The electrons confined in a quantum dot couple—in most cases quite weakly—to collective vibrations of the dot and its substrate.<sup>31</sup> In single-molecule devices, by contrast, the confined electrons interact

with local vibration modes of the molecule that can produce pronounced changes in the molecular electronic orbitals. Consequently, electron-phonon (e-ph) interactions are expected to play a much more important role in molecules than in quantum dots.

From the theoretical point of view, addressing both e-e and e-ph interactions from first principles is a very complicated task. However, simple effective models can provide good qualitative results, depending on the parameter regime and the method employed to solve the model Hamiltonian.<sup>26</sup> For example, the essential physics of certain experiments<sup>21,23</sup> appears to be described by variants of the Anderson-Holstein model, which augments the Anderson model<sup>32</sup> for a magnetic impurity in a metallic host with a Holstein coupling<sup>33</sup> of the impurity charge to a local phonon mode. The model has been studied since the 1970s in connection with other problems<sup>34-44</sup> prior to its application to single-molecule devices.<sup>45,46</sup> Various analytical approximations as well as nonperturbative numerical renormalization-group calculations have shown that in equilibrium, the Holstein coupling reduces the Coulomb repulsion between two electrons in the impurity level, even yielding effective e-e attraction for sufficiently strong e-ph coupling. Increasing the e-ph coupling from zero can produce a smooth crossover from a conventional Kondo effect, involving conduction-band screening of the impurity spin degree of freedom, to a charge Kondo effect in which it is the impurity “isospin” or deviation from half-filling that is quenched by the conduction band.

Single-molecule devices at finite bias are usually studied via nonequilibrium Keldysh Green's functions that systematically incorporate the many-body interactions within a system. Although this approach has proved to be the most reliable for calculation of transport properties, the results are highly sensitive to the approximations made. For instance, the equation-of-motion technique<sup>47</sup> generates a hierarchy of coupled equations for Green's functions containing  $2n$  fermionic operators

for  $n = 1, 2, 3, \dots$ : a hierarchy that must be decoupled at some level in order to become useful. The most commonly used decoupling scheme is based on a mean-field decomposition of the  $n = 2$  Green's functions, leading to the well-known Hubbard I approximation.<sup>48</sup> This approximation gives reasonable results for temperatures  $T$  above the system's Kondo temperature  $T_K$ , but as it neglects spin correlations between localized and conduction electrons, it fails in the Kondo regime.

A few years ago, two of us applied the equation-of-motion method decoupled at level  $n = 2$  to study a single-molecule junction that features phonon-assisted interorbital tunneling.<sup>49</sup> However, to capture the physics at  $T \lesssim T_K$  requires extension of the equation-of-motion hierarchy to higher order, which in most cases is carried out in the limit of infinite Coulomb interaction. The Kondo regime may also be studied via diagrammatic expansion within the non-crossing approximation, which is again most straightforward in the infinite-interaction limit.<sup>50</sup>

This paper reports the results of an investigation of the Kondo regime of a two-orbital molecule, with focus on situations in which Coulomb interactions are strong but finite. In order to treat e-e and e-ph interactions on an equal basis, we employ Wilson's numerical renormalization-group approach,<sup>51–53</sup> which allows complete access to the equilibrium behavior and linear response of the system for temperatures all the way to absolute zero. We show that the renormalization of e-e interactions is strongly dependent on the energy difference between the two molecular levels. For small interorbital energy differences, the renormalization is significantly enhanced compared with the situation of one active molecular orbital considered in previous work. This enhancement is detrimental for realization of the Kondo effect but improves the prospects for accessing a phonon-dominated regime of effective e-e attraction. A sharp crossover between Kondo to phonon-dominated regimes has signatures in thermodynamic properties and in charge transport across the molecule.

We note that we leave for future study cases involving two degenerate (or nearly degenerate) molecular orbitals lying below the chemical potential of the leads. In such cases, e-e interactions favor the presence of an unpaired electron in each orbital, and electron-phonon interactions may be expected to significantly affect the competition between total-spin-singlet and triplet ground states.<sup>54–56</sup>

The rest of the paper is organized as follows: Section II describes our model system and provides a preliminary analysis via canonical transformations. Section III summarizes the numerical solution method and Sec. IV presents the results. Concluding remarks appear in Sec. V.

## II. MODEL AND PRELIMINARY ANALYSIS

### A. Model Hamiltonian

We consider a system composed of a two-level molecule interacting with a local phonon mode and also coupled to two metallic leads, as shown schematically in Fig. 1. This system

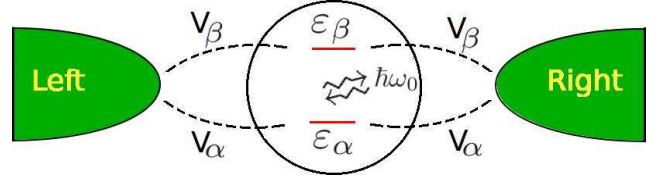


FIG. 1: (Color online) Schematic representation of the model studied in this work. A molecule with two active orbitals ( $\alpha$  and  $\beta$ ) spans the gap between left and right electrodes. The molecular orbitals are subject both to e-e and e-ph interactions.

is modeled by the Anderson-type Hamiltonian

$$H = H_{\text{mol}} + H_{\text{leads}} + H_{\text{mol-leads}}, \quad (1)$$

with  $H_{\text{mol}}$  describing the isolated molecule,  $H_{\text{leads}}$  modeling the leads, and  $H_{\text{mol-leads}}$  accounting for electron tunneling between the molecule and the leads.

The molecular Hamiltonian can in turn be divided into four parts:  $H_{\text{mol}} = H_{\text{e}} + H_{\text{ph}} + H_{\text{Hol}} + H_{\text{tun}}$ . Here, the electronic part

$$H_{\text{e}} = \sum_{i=\alpha,\beta} (\epsilon_i n_i + U_i n_{i\uparrow} n_{i\downarrow}) + U' n_{\alpha} n_{\beta}, \quad (2)$$

where  $n_{i\sigma} = d_{i\sigma}^\dagger d_{i\sigma}$  is the number operator for electrons of energy  $\epsilon_i$  and spin  $\sigma$  in molecular orbital  $i = \alpha$  or  $\beta$ ,  $n_i = n_{i\uparrow} + n_{i\downarrow}$ , and  $U_i$  and  $U'$  parametrize intraorbital and interorbital Coulomb repulsion, respectively. Without loss of generality, we take  $\epsilon_{\beta} \geq \epsilon_{\alpha}$ . The phonon part

$$H_{\text{ph}} = \hbar\omega_0 n_b \quad (3)$$

describes a dispersionless optical phonon mode of energy  $\hbar\omega_0$ , with  $n_b = b^\dagger b$ . The remaining two parts of  $H_{\text{mol}}$  describe two different types of e-ph interaction:

$$H_{\text{Hol}} = \lambda n_{\text{mol}} (b^\dagger + b) \quad (4)$$

is a Holstein coupling between the phonon displacement and the combined occupancy (i.e., charge)

$$n_{\text{mol}} = n_{\alpha} + n_{\beta} \quad (5)$$

of the two molecular orbitals, while

$$H_{\text{tun}} = \lambda' \sum_{\sigma} (d_{\alpha\sigma}^\dagger d_{\beta\sigma} + d_{\beta\sigma}^\dagger d_{\alpha\sigma}) (b^\dagger + b) \quad (6)$$

describes interorbital tunneling accompanied by emission or absorption of a phonon.

The left ( $\ell = L$ ) and right ( $\ell = R$ ) leads are represented by

$$H_{\text{leads}} = \sum_{\ell, \mathbf{k}, \sigma} \epsilon_{\mathbf{k}} c_{\ell\mathbf{k}\sigma}^\dagger c_{\ell\mathbf{k}\sigma}, \quad (7)$$

where  $c_{\ell\mathbf{k}\sigma}$  annihilates an electron with energy  $\epsilon_{\mathbf{k}}$ , wave vector  $\mathbf{k}$ , and spin  $\sigma$  in lead  $\ell$ . For simplicity, each lead is characterized by a flat density of states

$$\rho(\epsilon) = N_s^{-1} \sum_{\mathbf{k}} \delta(\epsilon - \epsilon_{\mathbf{k}}) = \frac{1}{2D} \Theta(D - |\epsilon|), \quad (8)$$

where  $N_s$  is the number of lattice sites in each lead,  $D$  is the half bandwidth and  $\Theta(x)$  is the Heaviside function.

Lastly,

$$H_{\text{mol-leads}} = \frac{1}{\sqrt{N_s}} \sum_{i=\alpha,\beta} \sum_{\ell,\mathbf{k},\sigma} (V_{\ell i} d_{i\sigma}^\dagger c_{\ell\mathbf{k}\sigma} + V_{i\ell} c_{\ell\mathbf{k}\sigma}^\dagger d_{i\sigma}) \quad (9)$$

describes tunneling between the molecular orbitals and the leads, allowing transport through the system. We assume that the tunneling matrix elements are real and have left-right symmetry so we can write  $V_{\ell i} = V_{i\ell} = V_i$ . Then it is useful to perform an even/odd transformation

$$c_{e\mathbf{k}\sigma} = \frac{1}{\sqrt{2}}(c_{R\mathbf{k}\sigma} + c_{L\mathbf{k}\sigma}) \quad (10)$$

$$c_{o\mathbf{k}\sigma} = \frac{1}{\sqrt{2}}(c_{R\mathbf{k}\sigma} - c_{L\mathbf{k}\sigma}), \quad (11)$$

which allows Eq. (9) to be rewritten

$$H_{\text{mol-leads}} = \sqrt{\frac{2}{N_s}} \sum_{i=\alpha,\beta} V_i \sum_{\mathbf{k},\sigma} (d_{i\sigma}^\dagger c_{e\mathbf{k}\sigma} + c_{e\mathbf{k}\sigma}^\dagger d_{i\sigma}), \quad (12)$$

With this transformation, the odd-parity degrees of freedom are fully decoupled from the molecular orbitals, and can safely be dropped. As a result, the problem reduces to one effective conduction channel described by a modified

$$H_{\text{leads}} = \sum_{\mathbf{k},\sigma} \varepsilon_{\mathbf{k}} c_{e\mathbf{k}\sigma}^\dagger c_{e\mathbf{k}\sigma}. \quad (13)$$

This channel is still described by the density of states in Eq. (8), and it imparts to molecular orbital  $i$  a width

$$\Gamma_i = \pi V_i^2 / D. \quad (14)$$

A similar transformation to an effective one-channel model can be derived in any situation where the tunneling matrix elements satisfy  $V_{L\alpha} V_{R\beta} = V_{L\beta} V_{R\alpha}$ , ensuring that both molecular orbitals couple to the same linear combination of left- and right-lead states.

Since this model of a two-orbital single-molecule junction contains eleven bare energy scales, we will focus our numerical calculations on a few examples that illustrate interesting physics, rather than attempting a complete exploration of the model's parameter space. It should be noted that in the limit where one of the molecular orbitals ( $\beta$ , say) is removed or becomes decoupled from the rest of the system, the model reduces to the Anderson-Holstein Hamiltonian studied previously.<sup>34-46</sup>

## B. Preliminary analysis via canonical transformation

Insight can be gained into the properties of the two-orbital model by performing a canonical transformation of the Lang-Firsov type<sup>57</sup> from the original Hamiltonian (1) to  $\tilde{H} =$

$e^{S_1} H e^{-S_1}$ . Following extensive algebra, it can be shown that the choice

$$S_1 = \frac{\lambda}{\hbar\omega_0} n_{\text{mol}} (b^\dagger - b) \quad (15)$$

eliminates the Holstein coupling between the local phonons and the molecular electron occupancy [Eq. (4)], leaving a transformed Hamiltonian

$$\tilde{H} = \tilde{H}_e + H_{\text{ph}} + \tilde{H}_{\text{tun}} + H_{\text{leads}} + \tilde{H}_{\text{mol-leads}}, \quad (16)$$

in which  $H_{\text{ph}}$  and  $H_{\text{leads}}$  remain as given in Eqs. (3) and (13), respectively;  $\tilde{H}_e$  has the same form as  $H_e$  [Eq. (2)] with the replacements

$$\varepsilon_i \rightarrow \tilde{\varepsilon}_i = \varepsilon_i - \lambda^2 / \hbar\omega_0, \quad (17a)$$

$$U_i \rightarrow \tilde{U}_i = U_i - 2\lambda^2 / \hbar\omega_0, \quad (17b)$$

$$U' \rightarrow \tilde{U}' = U' - 2\lambda^2 / \hbar\omega_0; \quad (17c)$$

the interorbital tunneling maps to

$$\tilde{H}_{\text{tun}} = \lambda' \sum_{\sigma} (d_{\alpha\sigma}^\dagger d_{\beta\sigma} + d_{\beta\sigma}^\dagger d_{\alpha\sigma}) \left[ b^\dagger + b - \frac{2\lambda}{\hbar\omega_0} (1 + n_{\alpha\bar{\sigma}} + n_{\beta\bar{\sigma}}) \right] \quad (18)$$

where  $\bar{\sigma} = -\sigma$ ; and the molecule-leads coupling term becomes

$$\tilde{H}_{\text{mol-leads}} = \sqrt{\frac{2}{N_s}} \sum_{i=\alpha,\beta} V_i \sum_{\mathbf{k},\sigma} (B_\lambda^\dagger d_{i\sigma}^\dagger c_{e\mathbf{k}\sigma} + B_\lambda c_{e\mathbf{k}\sigma}^\dagger d_{i\sigma}), \quad (19)$$

with

$$B_\varepsilon = \exp \left[ -\frac{\varepsilon}{\hbar\omega_0} (b^\dagger - b) \right] \equiv B_{-\varepsilon}^\dagger. \quad (20)$$

This transformation extends the one applied previously (e.g., see, Ref. 39) to the Anderson-Holstein model. It effectively eliminates the Holstein Hamiltonian term [Eq. (4)] by mapping the local phonon mode to a different displaced oscillator basis for each value of the total molecular occupancy  $n_{\text{mol}}$ , namely, the basis that minimizes the ground-state energy of  $H_e + H_{\text{ph}} + H_{\text{Hol}}$ . There are three compensating changes to the Hamiltonian: (1) Shifts in the orbital energies [Eq. (17a)] and, more notably, a reduction in the magnitude—or even a change in the sign—of each e-e interaction within the molecule [Eqs. (17b) and (17c)]. These renormalizations reflect the fact that the Holstein coupling lowers the energy of doubly occupied molecular orbitals relative to singly occupied and empty orbitals. This well-known effect underlies the standard e-ph mechanism for superconductivity. (2) Addition of correlated (molecular-occupation-dependent) interorbital tunneling [the  $\lambda$ -dependent term in Eq. (18)] to the phonon-assisted tunneling present in the original Hamiltonian. (3) Incorporation into the molecule-leads coupling [Eq. (19)] of operators  $B_\lambda$  and  $B_\lambda^\dagger$  that cause each electron tunneling event to be accompanied by the creation and absorption of a packet of phonons as the local bosonic mode adjusts to the change in the total molecular occupancy  $n_{\text{mol}}$ .

The effects of the phonon-assisted interorbital tunneling term  $H_{\text{tun}}$  can be qualitatively understood by rewriting Eq. (16) in terms of even and odd linear combinations of the  $\alpha$  and  $\beta$  molecular orbitals:

$$d_{e\sigma} = \frac{1}{\sqrt{2}}(d_{\alpha\sigma} + d_{\beta\sigma}), \quad d_{o\sigma} = \frac{1}{\sqrt{2}}(d_{\alpha\sigma} - d_{\beta\sigma}). \quad (21)$$

In this parity basis, Eq. (18) becomes

$$\tilde{H}_{\text{tun}} = \lambda' \sum_{\sigma} (n_{e\sigma} - n_{o\sigma}) \left[ b^{\dagger} + b - \frac{2\lambda}{\hbar\omega_0} (1 + n_{e\bar{\sigma}} + n_{o\bar{\sigma}}) \right], \quad (22)$$

where  $n_{p\sigma} = d_{p\sigma}^{\dagger} d_{p\sigma}$  for  $p = e$  or  $o$ . The phonon-assisted tunneling component of  $\tilde{H}_{\text{tun}}$  (i.e., the original  $H_{\text{tun}}$ ) can be eliminated by performing a second Lang-Firsov transformation

$$\hat{H} = e^{S_2} \tilde{H} e^{-S_2} \quad (23)$$

with

$$S_2 = \frac{\lambda'}{\hbar\omega_0} (n_e - n_o)(b^{\dagger} - b), \quad (24)$$

where  $n_p = n_{p\uparrow} + n_{p\downarrow}$ . Lengthy algebra reveals a transformed Hamiltonian

$$\hat{H} = \hat{H}_e + H_{\text{ph}} + H_{\text{leads}} + \hat{H}_{\text{mol-leads}}, \quad (25)$$

where

$$\begin{aligned} \hat{H}_e = & \sum_{p=e,o} (\tilde{\varepsilon}_p n_p + \tilde{U}_p n_{p\uparrow} n_{p\downarrow}) + \sum_{\sigma} (\tilde{U}_{\parallel} n_{e\sigma} n_{o\sigma} + \tilde{U}_{\perp} n_{e\sigma} n_{o\bar{\sigma}}) \\ & + \sum_{\sigma} [t + W(n_{e\bar{\sigma}} + n_{o\bar{\sigma}})] (B_{2\lambda'}^{\dagger} d_{e\sigma}^{\dagger} d_{o\sigma} + B_{2\lambda'} d_{o\sigma}^{\dagger} d_{e\sigma}) \\ & + J(S_e^{+} S_o^{-} + S_o^{+} S_e^{-} - B_{4\lambda'}^{\dagger} I_e^{+} I_o^{-} - B_{4\lambda'} I_e^{-} I_o^{+}) \end{aligned} \quad (26)$$

with  $S_p^{+} \equiv (S_p^{-})^{\dagger} = c_{p\uparrow}^{\dagger} c_{p\downarrow}$  and  $I_p^{+} \equiv (I_p^{-})^{\dagger} = c_{p\uparrow}^{\dagger} c_{p\downarrow}^{\dagger}$  being spin- and charge-raising operators, respectively, and

$$\hat{H}_{\text{mol-leads}} = \frac{2}{\sqrt{N_s}} \sum_{p=e,o} V_p \sum_{\mathbf{k},\sigma} (B_{\lambda+\lambda'}^{\dagger} d_{p\sigma}^{\dagger} c_{\mathbf{k}\sigma} + B_{\lambda+\lambda'} c_{\mathbf{k}\sigma}^{\dagger} d_{p\sigma}). \quad (27)$$

The renormalized parameters and operators entering Eqs. (26)

and (27) are

$$\tilde{\varepsilon}_p = \frac{\varepsilon_{\alpha} + \varepsilon_{\beta}}{2} - \frac{\lambda_p^2}{\hbar\omega_0}, \quad (28a)$$

$$\tilde{U}_p = \frac{2U' + U_{\alpha} + U_{\beta}}{4} - \frac{2\lambda_p^2}{\hbar\omega_0}, \quad (28b)$$

$$\tilde{U}_{\parallel} = U' - \frac{2\lambda_e \lambda_o}{\hbar\omega_0}, \quad (28c)$$

$$\tilde{U}_{\perp} = \frac{2U' + U_{\alpha} + U_{\beta}}{4} - \frac{2\lambda_e \lambda_o}{\hbar\omega_0}, \quad (28d)$$

$$t = \frac{\varepsilon_{\alpha} - \varepsilon_{\beta}}{2}, \quad (28e)$$

$$W = \frac{U_{\alpha} - U_{\beta}}{2}, \quad (28f)$$

$$J = \frac{2U' - U_{\alpha} - U_{\beta}}{4}, \quad (28g)$$

$$V_{e,o} = \frac{V_{\alpha} \pm V_{\beta}}{2}, \quad (28h)$$

where

$$\lambda_{e,o} = \lambda \pm \lambda'. \quad (29)$$

Since the e-e interactions are expressed much less compactly in the parity basis than in the original basis of  $\alpha$  and  $\beta$  orbitals, the elimination of the boson-assisted interorbital tunneling from the Hamiltonian comes at the price of much greater complexity in  $\hat{H}_e$  compared to  $H_e$  [Eq. (2)] and  $\tilde{H}_e$ . It is notable, though, that the e-e repulsion between two electrons within the even-parity [odd-parity] molecular orbital undergoes a non-negative reduction proportional to  $\lambda_e^2 = (\lambda + \lambda')^2$  [ $\lambda_o^2 = (\lambda - \lambda')^2$ ]. By contrast, the Coulomb repulsion between electrons in orbitals of different parity undergoes a shift proportional to  $-\lambda_e \lambda_o = \lambda'^2 - \lambda^2$  that may be of either sign. Whereas large values of  $|\lambda|$  favor double occupancy of both the  $\alpha$  and the  $\beta$  molecular orbital, large values of  $|\lambda'|$  favor double occupancy of either the  $e$  or the  $o$  linear combination [the degeneracy between these alternatives being broken by an amount  $(2\tilde{\varepsilon}_e + \tilde{U}_e) - (2\tilde{\varepsilon}_o + \tilde{U}_o) = -16\lambda\lambda'/\hbar\omega_0$ ]. Both limits yield a unique many-body ground state of a very different character than the spin-singlet Kondo state.

Since  $S_1$  defined in Eq. (15) can be rewritten  $S_1 = (\lambda/\hbar\omega_0)(n_e + n_o)(b^{\dagger} - b)$ , it commutes with  $S_2$  given in Eq. (24). As a result, the two Lang-Firsov transformations can be combined into a single canonical transformation

$$\hat{H} = e^S H e^{-S} \quad (30)$$

with

$$S = S_1 + S_2 = \frac{\lambda_e n_e + \lambda_o n_o}{\hbar\omega_0} (b^{\dagger} - b). \quad (31)$$

This canonical transformation maps the original phonon annihilation operator  $b$  to

$$\hat{b} = e^S b e^{-S} = b - \frac{\lambda_e n_e + \lambda_o n_o}{\hbar\omega_0}. \quad (32)$$



If the phonon energy  $\hbar\omega_0$  were to greatly exceed the thermal energy  $k_B T$  and all other energy scales within the model, the system's ground state would be expected to be characterized by  $\hat{b}^\dagger \hat{b} = 0$  and, hence,

$$\langle n_b \rangle \equiv \langle b^\dagger b \rangle = \left\langle \left( \frac{\lambda_e n_e + \lambda_o n_o}{\hbar\omega_0} \right)^2 \right\rangle. \quad (33)$$

However, the physical limit of greater interest is one in which the Coulomb interactions  $U_\alpha$ ,  $U_\beta$ , and  $U'$  are larger than  $\hbar\omega_0$ . The applicability of Eq. (33) to such situations is addressed in Sec. IV.

### III. NUMERICAL RENORMALIZATION-GROUP APPROACH

In order to obtain a robust description of the many-body physics of the model, we treat the Hamiltonian (1) using Wilson's numerical renormalization-group (NRG) method,<sup>51–53</sup> as extended to incorporate local bosonic degrees of freedom.<sup>41</sup> The effective conduction band formed by the even-parity combination of left- and right-lead electrons is divided into logarithmic bins spanning the energy ranges  $D\Lambda^{-(m+1)} < \pm\epsilon < D\Lambda^{-m}$  for  $m = 1, 2, 3, \dots$ , for some discretization parameter  $\Lambda > 1$ . After the continuum of band states within each bin is approximated by a single representative state (the linear combination of states within the bin that couples to the molecular orbitals), Eq. (13) is mapped via a Lanczos transformation to

$$H_{\text{leads}} \simeq \sum_{n=0}^{\infty} \sum_{\sigma} \tau_n (f_{n\sigma}^\dagger f_{n+1,\sigma} + f_{n+1,\sigma}^\dagger f_{n\sigma}), \quad (34)$$

representing a semi-infinite, nearest-neighbor tight-binding chain to which the impurity couples only at its end site  $n = 0$ . Since the hopping decays exponentially along the chain as  $\tau_n \sim D\Lambda^{-n/2}$ , the ground state can be obtained via an iterative procedure in which iteration  $N$  involves diagonalization of a finite chain spanning sites  $n \leq N$ . At the end of iteration  $N$ , a pre-determined number of low-lying many-body eigenstates is retained to form the basis for iteration  $N + 1$ , thereby allowing reliable access to the low-lying spectrum of chains containing tens or even hundreds of sites. See Ref. 53 for general details of the NRG procedure.

For our problem, NRG iteration  $N = 0$  treats a Hamiltonian  $H_0 = H_{\text{mol}} + H_{\text{mol-leads}}$ , with  $N_s^{-1/2} \sum_{\mathbf{k}} c_{e\mathbf{k}\sigma}$  in Eq. (12) replaced by  $\sqrt{2}f_{0\sigma}$ . Since the phonon mode described by  $H_{\text{ph}}$  has an infinite-dimensional Hilbert space, we must work in a truncated space in which the boson number is restricted to  $n_b \leq N_b$ .

#### A. Thermodynamic quantities

The NRG method can be used to evaluate a thermodynamic property  $X$  as

$$X(T) = \frac{1}{Z(T)} \sum_m \langle \Psi_m | X | \Psi_m \rangle e^{-\beta E_m}, \quad (35)$$

where  $|\Psi_m\rangle$  is a many-body eigenstate at iteration  $N$  having energy  $E_m$ ,  $\beta = 1/k_B T$ , and

$$Z(T) = \sum_m e^{-\beta E_m} \quad (36)$$

is the partition function evaluated at the same iteration. For a given value of  $N$ , Eqs. (35) and (36) provide a good account<sup>51–53</sup> of  $X(T)$  over a range of temperatures around  $T_N$  defined by  $k_B T_N = D\Lambda^{-N/2}$ .

For extensive properties  $X$ , it is useful to define the molecular contribution to the property as

$$X_{\text{mol}} = X_{\text{tot}} - X_{\text{leads}}, \quad (37)$$

where  $X_{\text{tot}}$  ( $X_{\text{leads}}$ ) is the total value of  $X$  for a system with (without) the molecule. In our problem, the local phonon mode is treated as part of the host system. Accordingly, we define the molecular entropy as

$$S_{\text{mol}}(T) = S_{\text{tot}}(T) - S_{\text{leads}}(T) - S_{\text{ph}}(T), \quad (38)$$

where  $S_{\text{tot}}(T)$  is the total entropy of the system,  $S_{\text{leads}}(T)$  is the contribution of the leads when isolated from the molecule, and  $S_{\text{ph}}(T)$  is the entropy of the truncated local-phonon system, given by

$$S_{\text{ph}}(T) = k_B [\ln Z_{\text{ph}}(T) - \partial \ln Z_{\text{ph}} / \partial \beta], \quad (39)$$

with

$$Z_{\text{ph}}(T) = \sum_{n_b=0}^{N_b} e^{-n_b \beta \hbar\omega_0} = \frac{1 - e^{-\beta \hbar\omega_0 (N_b + 1)}}{1 - e^{-\beta \hbar\omega_0}}. \quad (40)$$

Another property of interest is the molecular contribution to the static magnetic susceptibility,

$$\chi(T) = \frac{\beta(g\mu_B)^2}{Z(T)} \sum_m [\langle \Psi_m | S_z^2 | \Psi_m \rangle - |\langle \Psi_m | S_z | \Psi_m \rangle|^2] e^{-\beta E_m}, \quad (41)$$

where  $S_z$  is the total spin  $z$  operator,  $\mu_B$  is the Bohr magneton, and  $g$  is the Landé  $g$  factor (assumed to be the same for electrons in the leads and in the molecular orbitals). One can interpret  $|\mu_{\text{mol}}|^2 = 3Tk_B\chi_{\text{mol}}$  as the magnitude-squared of the molecule's effective magnetic moment.

#### B. Linear-response transport properties

In this paper, we restrict our calculations to equilibrium situations in which no external bias is applied. In such cases, inelastic transport produced by the e-ph interaction can be neglected<sup>58</sup> and the linear conductance through the molecule can be obtained from a Landauer-type formula

$$G(T) = G_0 \int_{-\infty}^{\infty} \left( -\frac{\partial f}{\partial \omega} \right) [-\text{Im} \mathcal{T}(\omega, T)] d\omega, \quad (42)$$

where

$$\mathcal{T}(\omega, T) = \frac{\pi}{2D} \sum_{i=\alpha,\beta} \sum_{\sigma} V_{Li} G_{ij}^{\sigma}(\omega, T) V_{jR}. \quad (43)$$

and  $G_0 = 2e^2/h$  is the quantum of conductance. The fully dressed retarded molecular Green's functions  $G_{ij}^\sigma(\omega, T)$  are defined by

$$G_{ij}^\sigma(\omega, T) = -i \int_0^\infty \langle [d_{i\sigma}(t), d_{j\sigma}^\dagger(0)]_+ \rangle e^{i(\omega+i\eta)t} dt, \quad (44)$$

where  $\langle \dots \rangle$  represents the equilibrium average in the grand canonical ensemble and  $\eta$  is a positive infinitesimal real number.

As shown for the related problem of two quantum dots connected in common to a pair of metallic leads,<sup>59</sup> in the case  $V_{li} = V_{il} = V_i$  assumed in the present work, Eq. (42) can be recast in the simpler form

$$G(T)/G_0 = \pi \Gamma_c \sum_\sigma \int_{-\infty}^\infty \left( -\frac{\partial f}{\partial \omega} \right) A_{cc}^\sigma(\omega, T) d\omega, \quad (45)$$

where  $\Gamma_c = \Gamma_\alpha + \Gamma_\beta$  and  $A_{cc}^\sigma(\omega, T) = \pi^{-1} \text{Im} G_{cc}^\sigma(\omega, T)$  [defined via Eq. (44)] is the spectral function for the current-carrying linear combination of the  $\alpha$  and  $\beta$  orbitals:

$$d_{c\sigma} = \sum_{i=\alpha,\beta} \sqrt{\Gamma_i/\Gamma_c} d_{i\sigma}. \quad (46)$$

Within the NRG approach, one can calculate

$$A_{cc}^\sigma(\omega, T) = \frac{1}{Z} \sum_{m,m'} |\langle \Psi_{m'} | d_{c\sigma}^\dagger | \Psi_m \rangle|^2 \left( e^{-\beta E_m} + e^{-\beta E_{m'}} \right) \times \delta_T(\omega - (E_{m'} - E_m)/\hbar), \quad (47)$$

where  $\delta_T(\omega)$  is a thermally broadened Dirac delta function.<sup>53</sup> We focus below exclusively on situations where there is no magnetic field, and hence  $A_{cc}^\sigma(\omega, T) = A_{cc}(\omega, T)$ , independent of  $\sigma$ .

#### IV. NUMERICAL RESULTS

This section presents NRG results obtained for the Hamiltonian defined by Eqs. (1)–(6), (12), and (13). We take the half bandwidth  $D = 1$  as our primary energy scale and adopt units in which  $\hbar = k_B = g\mu_B = 1$ . All results shown were obtained for the special case of equal orbital hybridizations  $V_\alpha = V_\beta = V$  and equal bare Coulomb repulsions  $U_\alpha = U_\beta = U' = U$ . These choices simplify several of the effective couplings entering Eq. (28), but qualitatively similar results are obtained for more general parameter choices. The calculations were performed for hybridization  $V = 0.075$  (hence,  $\Gamma = \pi V^2/D \simeq 0.0177$ ) and phonon energy  $\omega_0 = 0.1$  with NRG discretization parameter  $\Lambda = 2.5$ , allowing up to  $N_b = 60$  phonons in the local mode, and retaining 2 000–4 000 many-body states after each iteration.

##### A. Upper orbital far above chemical potential

We first consider the case of fixed  $\varepsilon_\beta = 4$  where the upper molecular orbital lies far above the chemical potential

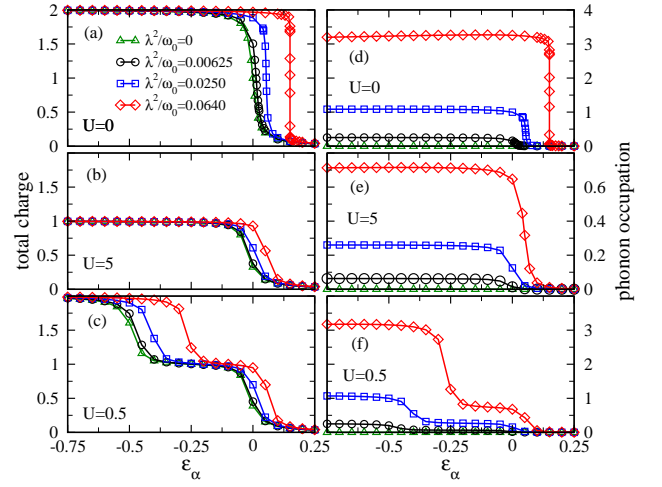


FIG. 2: (Color online) Variation with orbital energy  $\varepsilon_\alpha$  at zero temperature of (left) the charge  $\langle n_{\text{mol}} \rangle$ , and (right) the phonon occupation  $\langle n_b \rangle$ , for  $U = 0$  (top),  $U = 5$  (middle) and  $U = 0.5$  (bottom). Data are for  $\varepsilon_\beta = 4$ ,  $V = 0.075$ ,  $\lambda' = \lambda$ ,  $\omega_0 = 0.1$ , and the four values of  $\lambda^2/\omega_0$  listed in the legend.

of the leads and therefore contributes little to the low-energy physics. This situation, in which the two-orbital model largely reduces to the Anderson-Holstein model,<sup>34–46</sup> serves as a reference against which to compare cases in which both molecular orbitals are active. Given that the  $\beta$  orbital will have negligible occupation, the phonon-assisted interorbital tunneling  $H_{\text{tun}}$  is not expected to play a significant role. In Figs. 2 and 3 we show results obtained for  $\lambda' = \lambda$ . Figure 4 shows that almost identical properties arise for  $\lambda' = 0$ .

Figure 2 shows the total charge of the molecule and the phonon occupation as functions of  $\varepsilon_\alpha$ , calculated at  $T = 0$  for  $\lambda' = 0$ , four values of  $\lambda$ , and three values of  $U$ . First consider the case  $U = 0$  of vanishing e-e interactions shown in panels (a) and (d). For  $\lambda = 0$ ,  $\varepsilon_\alpha = 0$  is a point of degeneracy between configurations having molecular charges 0, 1, and 2;  $\langle n_{\text{mol}} \rangle$  increases from 0 to 2 over a narrow range  $\Delta\varepsilon_\alpha \simeq 4\Gamma$  as the  $\alpha$  orbital drops below the chemical potential of the leads. For  $\lambda > 0$ ,  $\tilde{U} = -2\lambda^2/\omega_0$  is negative, and the ground state switches from charge 0 to charge 2 around  $2\varepsilon_\alpha + \tilde{U} = 0$  or  $\varepsilon_\alpha = 2\lambda^2/\omega_0$ . There is a marked decrease in the step width  $\Delta\varepsilon_\alpha$  with increasing  $\lambda$  (to be discussed further below).

It is evident from Figs. 2(a) and 2(d) that changes in the ground-state phonon occupation are closely correlated with those in the total molecular charge. The prediction of Eq. (33) for the case  $\lambda' = \lambda$  (hence,  $\lambda_e = 2\lambda$  and  $\lambda_o = 0$ ) is  $\langle n_b \rangle = (2\lambda/\omega_0)^2 \langle n_e \rangle$ . Although this relation captures the correct trends in the variation of  $\langle n_b \rangle$  with  $\varepsilon_\alpha$  in Fig. 2(d), it overestimates the phonon occupation by a significant margin. Such deviations are not unexpected, given that Eq. (33) was derived under the assumption that  $\hbar\omega_0$  is the largest energy scale in the problem, whereas here  $\varepsilon_\beta$  is the dominant energy scale. Empirically, we find that  $\langle n_b \rangle$  lies closer to

$$\bar{n}_b = (2\lambda/\omega_0)^2 \langle n_e \rangle^2, \quad (48)$$

which also serves as a lower bound on the phonon occupation.

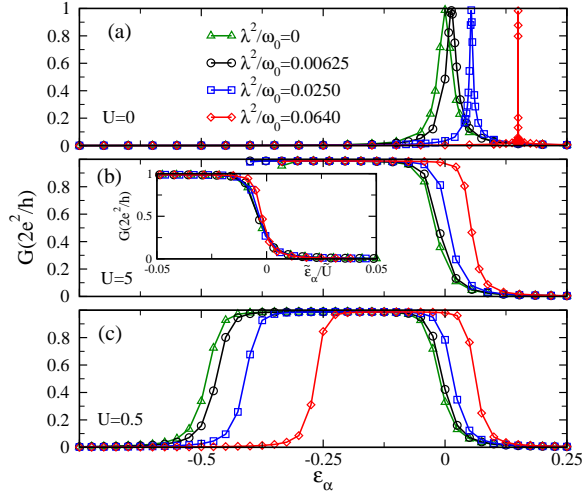


FIG. 3: (Color online) Zero-temperature conductance  $G$  vs orbital energy  $\varepsilon_\alpha$  for (a)  $U = 0$ , (b)  $U = 5$ , and (c)  $U = 0.5$ . Data are for  $\varepsilon_\beta = 4$ ,  $V = 0.075$ ,  $\lambda' = \lambda$ ,  $\omega_0 = 0.1$ , and the four values of  $\lambda^2/\omega_0$  listed in the legend. The inset in (b) shows the data from the main panel replotted as  $G$  vs  $\tilde{\varepsilon}_\alpha/\tilde{U}$ .

The error  $\langle n_b \rangle - \bar{n}_b$  is largest in the vicinity of the step in  $\langle n_{\text{mol}} \rangle$  and vanishes as  $\langle n_{\text{mol}} \rangle$  approaches 0 or 2. For  $\lambda^2/\omega_0 = 0.064$ ,  $\langle n_b \rangle - \bar{n}_b < 0.06$  both for  $\varepsilon_\alpha \leq 0.149$  and for  $\varepsilon_\alpha \geq 0.151$ , whereas for  $\varepsilon_\alpha = 0.149945$ ,  $\bar{n}_b \simeq 0.88$  underestimates  $\langle n_b \rangle$  by approximately 0.68. The peak error is smaller for the other e-ph couplings shown in Fig. 2(d).

For the case  $U = 5$  of very strong e-e interactions [Fig. 2(b) and 2(e)], the molecular charge rises from 0 to 1 around the point where  $\tilde{\varepsilon}_\alpha = 0$ . In contrast with the situation for  $U = 0$ , the step width  $\Delta\varepsilon_\alpha$  shows no appreciable change with  $\lambda$ . The phonon occupation across the charge-1 is described very well by Eq. (48).

Lastly, Figs. 2(c) and 2(f) show data for  $U = 0.5$ , exemplifying moderately strong e-e interactions. With decreasing  $\varepsilon_\alpha$  (at fixed  $\lambda$ ), the molecular charge rises in two steps, first from 0 to 1 as  $\tilde{\varepsilon}_\alpha$  decreases through the chemical potential, and then from 1 to 2 as  $\tilde{U} + \tilde{\varepsilon}_\alpha$  reaches zero. Just as for  $U = 5$ , each step has a width  $\Delta\varepsilon_\alpha = O(\Gamma)$  that is independent of  $\lambda$  over the range of e-ph couplings shown. The distance along the  $\varepsilon_\alpha$  axis between the two steps (i.e., the width of the charge-1 plateau), which is roughly  $\tilde{U} = U - 2\lambda^2/\omega_0$ , decreases as the e-ph coupling increases in magnitude. Away from the immediate vicinity of the charge steps, the phonon occupation is well-approximated by  $\bar{n}_b$  given in Eq. (48).

Figure 3 plots the zero-temperature linear conductance as a function of  $\varepsilon_\alpha$  for the same set of parameters as was used in Fig. 2. At  $T = 0$  in zero magnetic field, Eq. (45) reduces to  $G(T = 0)/G_0 = \pi\Gamma_c A_{cc}(0, 0)$ . In any regime of Fermi-liquid behavior,  $A_{cc}(0, 0)$  is expected to obey the Friedel sum-rule, implying that  $\pi\Gamma_c A_{cc}(0, 0) = 1$  in the wide-band limit where all other energy scales in the model are small compared with  $D$ . This property, which should hold even in the presence of

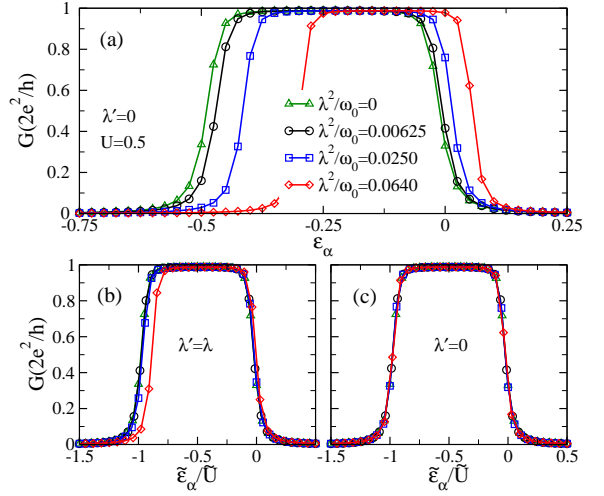


FIG. 4: (Color online) (a) Zero-temperature conductance  $G$  vs orbital energy  $\varepsilon_\alpha$  for the same parameters as used in Fig. 3(c), except here  $\lambda' = 0$ . (b) Data for  $\lambda' = \lambda$  from Fig. 3(c) replotted as  $G$  vs  $\tilde{\varepsilon}_\alpha/\tilde{U}$ . (c) Data for  $\lambda' = 0$  from (a) replotted as  $G$  vs  $\tilde{\varepsilon}_\alpha/\tilde{U}$ .

e-ph interactions within the molecule, leads to

$$G(T = 0) = G_0 \sin^2\left(\frac{\pi}{2}\langle n_{\text{mol}} \rangle\right). \quad (49)$$

For  $U = 0$  [Fig. 3(a)], we observe a conductance peak at the point of degeneracy between molecular charges 0 and 2. This is the noninteracting analog of the Coulomb blockade peak seen in strongly interacting quantum dots and single-molecule junctions above their Kondo temperatures. For  $\lambda = 0$ , the peak is located at  $\tilde{\varepsilon}_\alpha = \varepsilon_\alpha = 0$  and has a full width  $\Delta\varepsilon_\alpha \simeq 2\Gamma$ , as expected for this exactly solvable single-particle case. With increasing  $\lambda$ , the conductance peak shifts in position to  $\varepsilon_\alpha \simeq 2\lambda^2/\omega_0$  (the midpoint of the steps in  $\langle n_{\text{mol}} \rangle$  and  $\langle n_b \rangle$ ) while its width narrows, reflecting the same renormalization of  $\Gamma$  inferred from Figs. 2(a) and 2(d). For all values of  $\lambda$ , the maximum conductance is  $G = G_0$ , as predicted by Eq. (49) for the point where  $\langle n_{\text{mol}} \rangle$  passes through 1.

For the interacting cases shown in Figs. 3(b) and 3(c), the formation of a many-body Kondo resonance at the chemical potential leads to a near-unitary conductance at low-temperatures  $T \ll T_K$  over the entire range of  $\varepsilon_\alpha$  for which  $\langle n_{\text{mol}} \rangle \simeq 1$ . In the case  $U = 5$ , no data are shown for  $\varepsilon_\alpha \lesssim -0.4$ , a range in which the Kondo temperature  $T_K$  is so low that the ground-state properties are experimentally inaccessible. For both  $U = 0.5$  and  $U = 5$ , the conductance data show quite good collapse when plotted against  $\tilde{\varepsilon}_\alpha/\tilde{U}$  [see Fig. 3(b) inset and Fig. 4(b), respectively]. This scaling confirms that the main features are associated with the conditions  $\tilde{\varepsilon}_\alpha = 0$  and  $\tilde{\varepsilon}_\alpha = -\tilde{U}$ .

It has already been remarked that the phonon-assisted interorbital tunneling is expected to play little role in cases where the  $\beta$  orbital is far above the Fermi energy. To investigate this issue, we have compared data for  $\lambda' = \lambda$  and  $\lambda' = 0$  with all other parameters the same. The molecular charge and the phonon occupation are virtually indistinguishable in the

two cases. The conductance curves are also very similar, as exemplified for  $U = 0.5$  by Figs. 3(c) and 4(a). However, there are subtle differences that can be highlighted by replotting  $G$  against the scaling variable  $\tilde{\varepsilon}_\alpha/\tilde{U}$ . The conductance steps in the  $\lambda' = \lambda$  data [Fig. 4(b)] conform well to the conditions  $\tilde{\varepsilon}_\alpha = 0$  and  $\tilde{\varepsilon}_\alpha = -\tilde{U}$ , but the collapse is even better in the case  $\lambda' = 0$  [Fig. 4(c)].

We conclude this discussion of situations in which the  $\beta$  molecular level lies far above the chemical potential by returning to the narrowing with increasing  $\lambda$  at  $U = 0$  of the steps in the molecular charge and the phonon occupancy, and of the peaks in the linear conductance. This behavior is associated with the presence of a direct crossover of  $\langle n_{\text{mol}} \rangle$  from 0 to 2, as opposed to distinct crossovers from 0 to 1, then from 1 to 2. The same step narrowing can be seen for  $U > 0$  when  $\lambda$  becomes large enough to suppress the  $\langle n_{\text{mol}} \rangle = 1$  plateau. (For  $U = 0.5$  and  $\lambda' = \lambda$ , this takes place around  $\lambda^2/\omega_0 = 0.15$ , considerably larger than any of the values shown in Figs. 2 and 3.)

### B. Both orbitals near the chemical potential

The rich behavior of the model described by Eqs. (1)–(9) becomes apparent only in the regime where both molecular orbitals lie close to the chemical potential and therefore can contribute to the low-energy physics. We focus on situations in which the orbitals are arranged symmetrically around the chemical potential, i.e.,  $\varepsilon_\beta = -\varepsilon_\alpha = \delta \geq 0$ , a small energy scale. (Other arrangements are briefly considered at the end of the subsection.) For simplicity, we take  $\lambda' = \lambda$  throughout.

We begin by using the transformed Hamiltonian  $\hat{H}$  defined in Eq. (25) to calculate the energies of the low-lying states of the isolated molecule in the absence of any electron tunneling to/from the leads (i.e., for  $V = 0$ ). As in the previous subsection, we take  $U_\alpha = U_\beta = U' = U$ , a condition that ensures  $J = W = 0$ ,  $U_\perp = U_\parallel$ , and  $t = -\delta$  in Eq. (26). Then the only explicit e-ph coupling remaining in  $\hat{H}$  appears in the term  $t \sum_\sigma (B_{2\lambda'}^\dagger c_{e\sigma}^\dagger c_{o\sigma} + \text{H.c.})$ . Since  $|t| = \delta$  is small, this Hamiltonian term causes only a weak admixture of states with nonzero phonon occupancy into the ground state. We therefore focus on the low-lying states of  $P_0 \hat{H}_e P_0$ , where  $\hat{H}_e$  given in Eq. (26) is the pure-electronic part of  $\hat{H}$  and  $P_0$  projects into the zero-phonon sector of the Fock space. Table I lists the low-lying energy eigenstates in this sector for the case  $\delta = 0$  where both the  $\alpha$  and the  $\beta$  molecular orbital lie precisely at the chemical potential. Also listed are the energies of these states including the leading perturbative corrections for  $\delta > 0$ . These corrections contain a multiplicative factor  $|\langle 0|B_{\pm 2\lambda'}|0\rangle|^2 = \exp[-4(\lambda/\omega_0)^2]$  reflecting the reduction with increasing e-ph coupling of the overlap of the phonon ground states for Fock-space sectors of different  $n_{\text{mol}}$ .

It can be seen from Table I that the singly occupied states of lowest energy are  $|\phi_1^{(1)}\rangle$  and  $|\phi_2^{(1)}\rangle$ , while the doubly occupied state of lowest energy is  $|\phi_1^{(2)}\rangle$ . One can use the energies of

$n_{\text{mol}}$	state, $ \phi_i^{(n_{\text{mol}})}\rangle$	energy, $E_i^{(n_{\text{mol}})}$
0	$ \phi_1^{(0)}\rangle =  0\rangle$	$E_1^{(0)} = 0$
1	$ \phi_1^{(1)}\rangle = d_{e\uparrow}^\dagger  0\rangle$	$E_1^{(1)} = -4x - \frac{1}{4}y$
	$ \phi_2^{(1)}\rangle = d_{e\downarrow}^\dagger  0\rangle$	$E_2^{(1)} = -4x - \frac{1}{4}y$
	$ \phi_3^{(1)}\rangle = d_{o\uparrow}^\dagger  0\rangle$	$E_3^{(1)} = \frac{1}{4}y$
	$ \phi_4^{(1)}\rangle = d_{o\downarrow}^\dagger  0\rangle$	$E_4^{(1)} = \frac{1}{4}y$
2	$ \phi_1^{(2)}\rangle = d_{e\uparrow}^\dagger d_{e\downarrow}^\dagger  0\rangle$	$E_1^{(2)} = U - 16x - \frac{1}{6}y$
	$ \phi_2^{(2)}\rangle = d_{e\uparrow}^\dagger d_{o\downarrow}^\dagger  0\rangle$	$E_2^{(2)} = U - 4x - \frac{1}{6}y$
	$ \phi_3^{(2)}\rangle = d_{e\downarrow}^\dagger d_{o\uparrow}^\dagger  0\rangle$	$E_3^{(2)} = U - 4x - \frac{1}{6}y$
	$ \phi_4^{(2)}\rangle = d_{e\uparrow}^\dagger d_{o\uparrow}^\dagger  0\rangle$	$E_4^{(2)} = U - 4x$
	$ \phi_5^{(2)}\rangle = d_{e\downarrow}^\dagger d_{o\downarrow}^\dagger  0\rangle$	$E_5^{(2)} = U - 4x$
	$ \phi_6^{(2)}\rangle = d_{o\uparrow}^\dagger d_{o\downarrow}^\dagger  0\rangle$	$E_6^{(2)} = U + \frac{1}{2}y$

TABLE I: Low-lying eigenstates  $|\phi_i^{(n_{\text{mol}})}\rangle$  of  $P_0 \hat{H}_e P_0$  where  $\hat{H}_e$  is defined in Eq. (26) and  $P_0$  is a projection operator into the zero-phonon sector of the Fock space. Eigenstates for  $\delta = \varepsilon_\beta = -\varepsilon_\alpha = 0$ ,  $U_\alpha = U_\beta = U' = U$ , and  $\lambda' = \lambda > 0$  are grouped according to their total electron number  $n_{\text{mol}}$ , and specified in terms of operators  $d_{p\sigma}^\dagger$  defined in Eqs. (21) acting on  $|0\rangle$ , the vacuum state for electrons and phonons.  $E_i^{(n_{\text{mol}})}$  is the energy of state  $|\phi_i^{(n_{\text{mol}})}\rangle$  including the leading perturbative correction for  $\delta > 0$ , expressed in terms of  $U$ ,  $x = \lambda^2/\omega_0$ , and  $y = \omega_0(\delta/\lambda)^2 \exp[-4(\lambda/\omega_0)^2]$ . (The nondegenerate perturbation theory used to derive the energies is valid only for  $\lambda \neq 0$ .)

these states to define an effective Coulomb interaction

$$U_{\text{eff}} = E_1^{(2)} - 2E_1^{(1)} = U - \frac{8\lambda^2}{\omega_0} + \frac{\delta^2 \omega_0}{3\lambda^2} \exp[-4(\lambda/\omega_0)^2]. \quad (50)$$

In the limit of small  $\delta$ , this value decreases with increasing  $\lambda^2/\omega_0$  at a rate four times greater than the effective Coulomb interaction  $\tilde{U}_\alpha$  [Eq. (17b)] in the  $\alpha$  level when the  $\beta$  level is far above the chemical potential. This property of molecules having multiple, nearly-degenerate orbitals enhances the prospects of attaining a regime of negative  $U_{\text{eff}}$  and may have interesting consequences in the area of superconductivity.

Table I also indicates that the ground state of the isolated molecule crosses from single electron occupancy (for smaller  $|\lambda|$ ) to double occupancy (for larger  $|\lambda|$ ) at an e-ph coupling determined by the condition  $E_1^{(2)} = E_1^{(1)}$ , which yields  $\lambda^2/\omega_0 = (U/12)[1 + O(\delta^2/U^2)]$ . As will be discussed in the paragraphs that follow, a similar crossing that takes place in the full problem with nonvanishing coupling between the molecule and the leads results in pronounced changes in the system's low-temperature properties. Since the lowest energy of a state having  $n_{\text{mol}} > 2$  (not shown in Table I) is  $3U - 16x - y/12$  (which exceeds  $E_1^{(2)}$  by at least  $2U$ ), such states play no role in the low-energy physics.

Figure 5(a) shows the evolution of the zero-temperature molecular charge  $\langle n_{\text{mol}} \rangle$  with  $\lambda^2/\omega_0$  for  $U = 0.5$  and four values of  $\delta$  satisfying  $\delta \ll U$ , while Fig. 6 presents the corresponding occupancies of individual molecular orbitals:  $\langle n_\alpha \rangle$



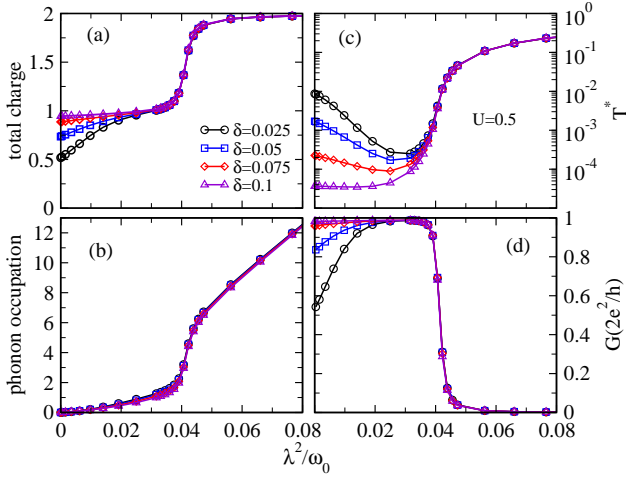


FIG. 5: (Color online) Variation with  $\lambda^2/\omega_0$  of (a) the ground-state molecular charge  $\langle n_{\text{mol}} \rangle = \langle n_e \rangle + \langle n_o \rangle$ , (b) the ground-state phonon occupation  $\langle n_b \rangle$ , (c) the crossover temperature  $T^*$ , and (d) the zero-temperature linear conductance  $G$ , all calculated for  $U = 0.5$ ,  $V = 0.075$ ,  $\omega_0 = 0.1$ , and the four values of  $\delta = \varepsilon_\beta = -\varepsilon_\alpha$  listed in the

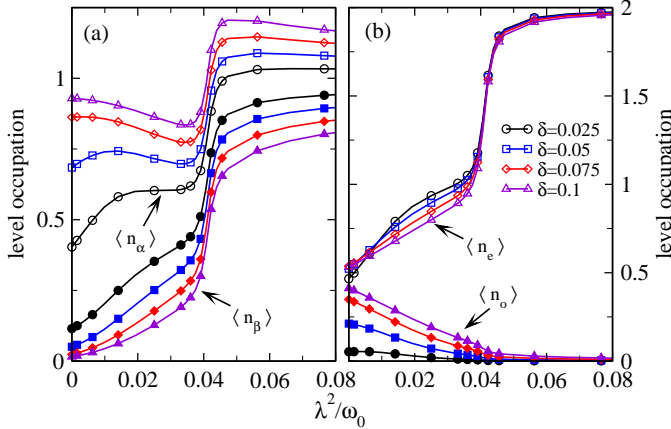


FIG. 6: (Color online) Occupation of individual molecular orbitals vs  $\lambda^2/\omega_0$  for  $U = 0.5$ ,  $V = 0.075$ ,  $\omega_0 = 0.1$ , and the four values of  $\delta = \varepsilon_\beta = -\varepsilon_\alpha$  listed in the legend: (a)  $\langle n_\alpha \rangle$  (open symbols) and  $\langle n_\beta \rangle$  (filled symbols); (b)  $\langle n_e \rangle$  (open symbols) and  $\langle n_o \rangle$  (filled symbols).

and  $\langle n_\beta \rangle$  in panel (a), and  $\langle n_e \rangle$  and  $\langle n_o \rangle$  in panel (b). We begin by considering the special case  $\lambda = 0$  in which the electron and phonon subsystems are entirely decoupled. For  $\delta \ll \Gamma = \pi V^2/D \simeq 0.0177$ ,  $\langle n_{\text{mol}} \rangle \simeq \langle n_e \rangle \simeq 0.5$ , which may be understood as a consequence of the ground state being close to that for  $U = V = \infty$  and  $\delta = 0$ : a product of (1)  $\frac{1}{2}[c_{e\uparrow}^\dagger d_{e\downarrow}^\dagger - c_{e\downarrow}^\dagger d_{e\uparrow}^\dagger - \sqrt{2}c_{e\uparrow}^\dagger c_{e\downarrow}^\dagger]|0\rangle$  where  $c_{e\sigma} = (2N_s)^{-1/2} \sum_{\mathbf{k}} c_{e\mathbf{k}\sigma}$  annihilates an electron in the linear combination of left- and right-lead states that tunnels into/out of the molecular orbitals, and (2) other lead degrees of freedom that are decoupled from the molecule. The total charge increases with  $\delta$  and approaches  $\langle n_{\text{mol}} \rangle = \langle n_\alpha \rangle = 1$  for  $\delta \gg \Gamma$ , in which limit the large Coulomb repulsion  $U$  leads to local-moment formation

in the  $\alpha$  orbital. The local moment is collectively quenched by lead electrons, leading to a Kondo singlet ground state. Figure 5(c) shows the characteristic temperature  $T^*$  of the quenching of the molecular spin degree of freedom, determined via the standard criterion<sup>51</sup>  $T^* \chi_{\text{mol}}(T^*) = 0.0701$ . This temperature is of order  $\Gamma$  in the mixed-valence limit  $\delta \ll \Gamma$ , but is exponentially reduced in the local-moment regime  $\delta \gg \Gamma$  where  $T^*$  represents the system's Kondo scale.

Turning on e-ph couplings  $\lambda' = \lambda$  lowers the energy of the even-parity molecular orbital below that of the odd orbital, and initially drives the system toward  $\langle n_e \rangle = 1$ ,  $\langle n_o \rangle = 0$ , and toward a many-body singlet ground state formed between the leads and a local moment in the even-parity molecular orbital.  $T^*$  in Fig. 5(c) shows an initial decrease with increasing  $\lambda^2/\omega_0$  that is very strong for the smaller values for  $\delta$ , where the e-ph coupling drives the system from mixed valence into the Kondo regime. For larger  $\delta$ , where the system is in the Kondo limit even at  $\lambda = 0$ , there is a much milder reduction of  $T^*$  caused by the phonon-induced shift of the filled molecular orbital further below the chemical potential.

Upon further increase in the e-ph coupling,  $\langle n_{\text{mol}} \rangle$  and  $T^*$  both show rapid but continuous rises around some value  $\lambda = \lambda_x$ . The crossover value  $\lambda_x^2/\omega_0 \simeq 0.042$ , which is independent of  $\delta$  for  $\delta \ll U$ , coincides closely with its  $\delta \rightarrow 0$  value  $U/12 \simeq 0.0417$  for the isolated molecule, where it describes the crossing of the singly occupied state  $|\psi_1^{(1)}\rangle$  and the doubly occupied state  $|\psi_1^{(2)}\rangle$  (see Table I). For  $\Gamma > 0$ , the corresponding energies  $E_1^{(1)}$  and  $E_1^{(2)}$  each acquire a half width  $\Gamma$  so the crossover of the ground-state molecular charge from 1 to 2 is smeared over the range  $|U - 12\lambda^2/\omega_0| \lesssim 2\Gamma$ . This implies a full width for the crossover  $\Delta(\lambda^2/\omega_0) \simeq 4\Gamma/12 = 0.006$ , an estimate in good agreement with Figs. 5(a) and 6.

In the regime  $\lambda \gtrsim \lambda_x$ , minimization of the e-ph energy through  $\langle n_e \rangle \simeq 2$ ,  $\langle n_o \rangle \simeq 0$  (shown in Fig. 6 to hold for all the  $\delta$  values considered) outweighs the benefits of forming a many-body Kondo singlet. Therefore,  $T^*$  characterizing the vanishing of  $T\chi_{\text{mol}}$  ceases to represent the Kondo temperature and instead characterizes the scale, of order  $12\lambda^2/\omega_0 - U$ , at which deviations of the molecular occupancies from their ground-state values become frozen out.

Over the entire range of  $\delta$  and  $\lambda^2/\omega_0$  illustrated in Figs. 5 and 6, the ground-state phonon occupation  $\langle n_b \rangle$  [Fig. 5(b)] closely tracks  $\bar{n}_b$  defined in Eq. (48) to within an absolute error  $0 \leq \langle n_b \rangle - \bar{n}_b \leq 0.2$ , an error that peaks around  $\lambda = \lambda_x$ . Similarly, the  $T = 0$  conductance [Fig. 5(d)] is everywhere well-described by Eq. (49), reaching the unitary limit  $G_0$  over a window of Kondo behavior for  $\lambda \lesssim \lambda_x$  in which the molecular occupancy is 1, then plunging to zero as the Kondo effect is destroyed and the occupancy rises to 2.

We note that the equilibrium properties shown in Figs. 5 and 6 exhibit no special features in the resonant case  $\delta = 0.05$  in which the molecular level spacing  $\varepsilon_\beta - \varepsilon_\alpha$  exactly matches the phonon energy. We expect the resonance condition to play a significant role only in driven setups where a nonequilibrium phonon distribution serves as a net source or sink of energy for the electron subsystem.

To this point, we have focused entirely on ground-state ( $T = 0$ ) properties. We now briefly discuss the finite-

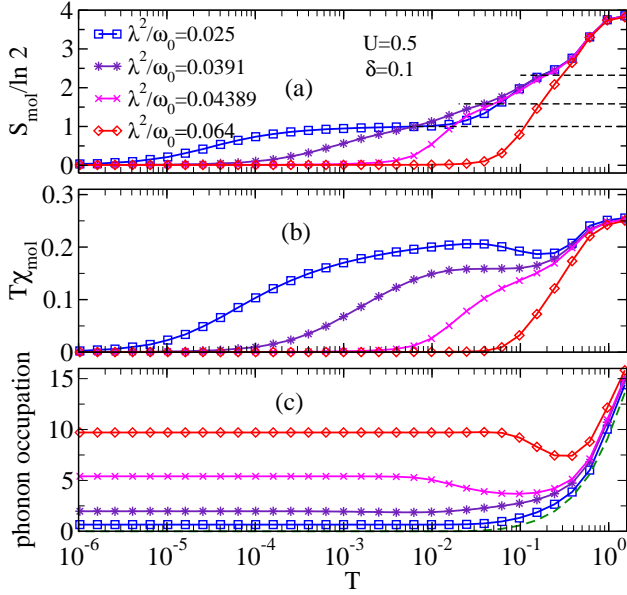


FIG. 7: (Color online) Temperature dependence of (a) the molecular entropy, (b) temperature times the molecular susceptibility,  $T\chi_{\text{mol}} \equiv |\mu_{\text{mol}}|^2/3$ , where  $\mu_{\text{mol}}$  is the molecule's magnetic moment, and (c) the phonon occupation. Data for  $U = 0.5$ ,  $\delta = 0.1$ ,  $V = 0.075$  and the four values of  $\lambda^2/\omega_0$  listed in the legend. In (a), the horizontal dashed lines mark  $S_{\text{mol}} = \ln 2$ ,  $\ln 3$ , and  $\ln 5$ . In (c), the dashed line shows the occupation of a free phonon mode of energy  $\omega_0 = 0.1$ .

temperature behavior in situations where the molecular orbitals are arranged symmetrically around the chemical potential. Figure 7 plots the temperature dependence of the molecular entropy, molecular susceptibility, and phonon occupation for  $U = 0.5$ ,  $\delta = 0.1$ ,  $V = 0.075$ , and four different values of  $\lambda^2/\omega_0$ . As long as the temperature exceeds all molecular energy scales, the entropy and susceptibility are close to the values  $S_{\text{mol}} = \ln 4$  and  $T\chi_{\text{mol}} = 1/8$  attained when every one of the 16 molecular configurations has equal occupation probability, while the phonon occupation is close to the Bose-Einstein result for a free boson mode of energy  $\omega_0$  [dashed line in Fig. 7(c)]. Once the temperature drops below  $U$ , most of the molecular configurations (and all with total charge  $n_{\text{mol}} > 2$ ) become frozen out. For  $\lambda \ll \lambda_x$  (exemplified by  $\lambda^2/\omega_0 = 0.025$  in Fig. 7), there is a slight shoulder in the entropy around  $S_{\text{mol}} = \ln 5$  and a minimum in the square of the local moment around  $T\chi_{\text{mol}} = 1/5$ , the values expected when the empty and singly occupied molecular configurations (the first five states listed in Table I are quasidegenerate. At lower temperatures, there is an extended range of local-moment behavior ( $S_{\text{mol}} = \ln 2$ ,  $T\chi_{\text{mol}} \approx 1/4$ ) associated with single occupancy of the even-parity molecular level (states  $|\phi_1^{(1)}\rangle$  and  $|\phi_2^{(1)}\rangle$ ). Finally, the properties cross over below the temperature scale  $T^*$  defined above to those of the Kondo singlet state:  $S_{\text{mol}} = 0$ ,  $T\chi_{\text{mol}} = 0$ .

For  $\lambda$  just below  $\lambda_x$  ( $\lambda^2/\omega_0 = 0.0391$  in Fig. 7) there are weak shoulders near  $S_{\text{mol}} = \ln 5$  and  $T\chi_{\text{mol}} = 1/5$ , as in the limit of smaller e-ph couplings. In this case, however, these features reflect the near degeneracy of the four  $n_{\text{mol}} = 1$

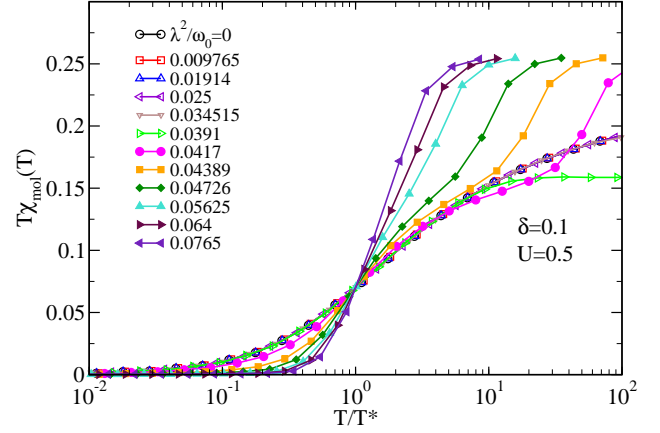


FIG. 8: (Color online) Magnetic moment  $\mu^2 = T\chi_{\text{mol}}$  vs scaled temperature  $T/T^*$  for  $U = 0.5$ ,  $\delta = 0.1$ ,  $V = 0.075$  and values of  $\lambda^2/\omega_0$  spanning the crossover from the Kondo regime to the doubly occupied regime. The collapse over the range  $T \lesssim 10T^*$  of all curves corresponding to  $\lambda^2/\omega_0 \leq 0.0391$  demonstrates the universal physics of the Kondo regime. No such universality is present in the boson-dominated limit.

configurations and the lowest-energy  $n_{\text{mol}} = 2$  configuration:  $|\phi_1^{(2)}\rangle$  in Table I. At slightly lower temperatures, the states  $|\phi_3^{(1)}\rangle$  and  $|\phi_4^{(1)}\rangle$  become depopulated and the properties drop through  $S_{\text{mol}} = \ln 3$  and  $T\chi_{\text{mol}} = 1/6$  before finally falling smoothly to zero. Even though there is no extended regime of local-moment behavior, the asymptotic approach of  $S_{\text{mol}}$  and  $T\chi_{\text{mol}}$  to their ground state values is essentially identical to that for  $\lambda \ll \lambda_x$  after rescaling of the temperature by  $T^*$ . As shown in Fig. 8, throughout the regime  $\lambda < \lambda_x$ ,  $T\chi_{\text{mol}}$  follows the same function of  $T/T^*$  for  $T \lesssim 10T^*$ . This is just one manifestation of the universality of the Kondo regime, in which  $T_K \equiv T^*$  serves as the sole low-energy scale.

A small increase in  $\lambda^2/\omega_0$  from 0.0391 to 0.04389, slightly above  $\lambda_x^2/\omega_0 = 0.0417$ , brings about significant changes in the low-temperature properties. While there are still weak features in the entropy at  $\ln 5$  and  $\ln 3$ , the final approach to the ground state is more rapid than for  $\lambda < \lambda_x$ , as can be seen from Fig. 8. Note also the upturn in  $\langle n_b \rangle$  as  $T$  falls below about  $10T^*$ —a feature absent for  $\lambda < \lambda_x$  that signals the integral role played by phonons in quenching the molecular magnetic moment.

Finally, in the limit  $\lambda \gg \lambda_x$  (exemplified by  $\lambda^2/\omega_0 = 0.064$  in Fig. 7),  $E_1^{(2)}$  is by a considerable margin the lowest eigenvalue of  $P_0 \hat{H}_e P_0$ , so with decreasing temperature  $S_{\text{mol}}$  and  $T\chi_{\text{mol}}$  quickly approach zero with little sign of any intermediate regime. Even though the quenching of the molecular degrees of freedom arises from phonon-induced shifts in the molecular levels rather than from a many-body Kondo effect involving strong entanglement with the lead degrees, the  $\lambda \rightarrow \infty$  ground state is adiabatically connected to that for  $\lambda = 0$ .

To conclude this subsection, we consider the effect of shifting the two molecular levels at a fixed, small energy separation  $\varepsilon_\beta - \varepsilon_\alpha = 2\delta$  through the application of a gate voltage  $V_g$  that

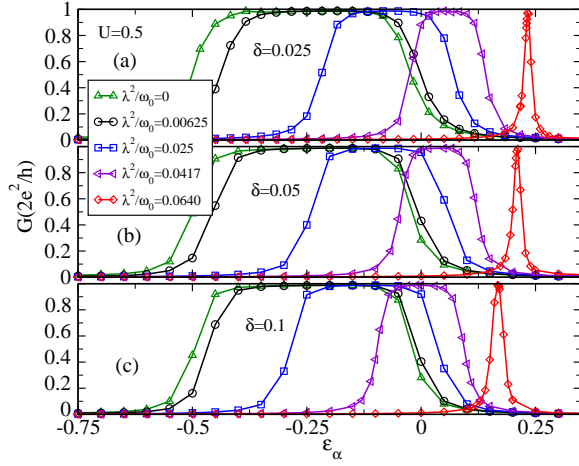


FIG. 9: (Color online) Zero-temperature conductance  $G$  as a function of  $\varepsilon_\alpha = -\delta - V_g$  (where  $V_g$  is an applied gate voltage) for the five values of  $\lambda^2/\omega_0$  listed in the legend and (a)  $\delta = 0.025$ , (b)  $\delta = 0.05$ , and (c)  $\delta = 0.1$ . The other parameters are  $U = 0.5$ ,  $V = 0.075$ , and  $\omega_0 = 0.1$ .

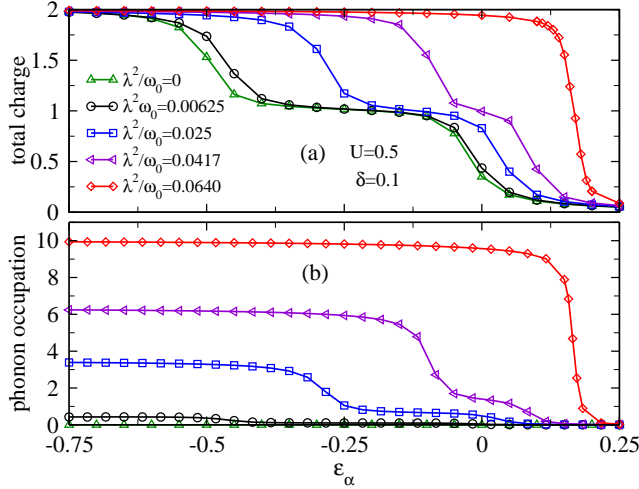


FIG. 10: (Color online) (a) Ground-state molecular charge and (b) ground-state phonon occupation as functions of  $\varepsilon_\alpha = -\delta - V_g$  (where  $V_g$  is an applied gate voltage) for  $\delta = 0.1$  and the values of  $\lambda^2/\omega_0$  listed in the legend. The other parameters are  $U = 0.5$ ,  $V = 0.075$ , and  $\omega_0 = 0.1$ .

causes  $\varepsilon_i$  in Eq. (2) to be replaced by  $\varepsilon_i - eV_g$ , and  $\tilde{\varepsilon}_p$  in Eq. (26) to be replaced by  $\tilde{\varepsilon}_p - eV_g$ . Figure 9 plots the gate-voltage dependence of the linear conductance for  $U = 0.5$ , five values of  $\lambda' = \lambda$ , and for  $\delta = 0.025$  [panel (a)],  $\delta = 0.05$  (b), and  $\delta = 0.1$  (c). Figure 10 shows the corresponding evolution of the total molecular charge and the phonon occupation for the case  $\delta = 0.1$ . In both figures, the quantity plotted along the horizontal axis is  $\varepsilon_\alpha = -\delta - eV_g$ , which allows direct comparison with the results shown in in Figs. 2(c), 2(f), and 3(c) for the regime where the  $\beta$  molecular orbital lies far above the chemical potential.

Just as in the other situations considered above, the zero-temperature conductance obeys the Fermi-liquid relation Eq.

(49). A plateau at  $G \approx G_0$  spans the range of gate voltages within which the total molecular occupancy is  $\langle n_{\text{mol}} \rangle \approx 1$  [e.g., compare Figs. 9(c) and 10(a)], while the conductance approaches zero for larger  $V_g$ , where the molecular charge vanishes, and for smaller  $V_g$ , where  $\langle n_{\text{mol}} \rangle \approx 2$ .

Once again, we begin by considering the limit  $\lambda = 0$  of zero e-ph coupling. For  $\delta = 0.025 \ll \Gamma = 0.0177$ , the steps between zero and peak conductance are somewhat broader (along the  $\varepsilon_\alpha$  axis) than their counterparts in cases where the  $\beta$  molecular orbital lies far above the chemical potential [compare with Fig. 3(c)]. This broadening can be understood as a consequence of the step in  $\langle n_{\text{mol}} \rangle$  being split into changes in  $\langle n_\alpha \rangle$  and in  $\langle n_\beta \rangle$ . When  $\delta \gg \Gamma$ , the  $\beta$  molecular level is essentially depopulated [as can be seen for the  $V_g = 0$  in Fig. 6(a)] and the conductance steps narrow to a width similar to that for  $\varepsilon_\beta = 4$ .

Increase of the e-ph coupling from zero results in shifts of the occupancy and conductance steps to progressively higher values of  $\varepsilon_\alpha$  (or to lower values of  $V_g$ ) that can be attributed to the phonon-induced renormalization of the orbital energies and of the Coulomb interactions. For  $\delta = 0.025$ , the width of the  $\langle n_{\text{mol}} \rangle \approx 1$ ,  $G \approx G_0$  plateau is close to the value  $U_{\text{eff}}$  defined in Eq. 50, which approaches  $U - 8\lambda^2/\omega_0$  in the limit  $\delta \lesssim \lambda^2/\omega_0$  satisfied by the  $\delta = 0.025$  curves in Eq. 9(a). Even for the  $\delta = 0.1$  curves shown in Fig. 9(b), the plateau width is at least  $U - 8\lambda^2/\omega_0$ , considerably larger than its value  $\tilde{U} = U - 2\lambda^2/\omega_0$  when the orbital  $\beta$  lies far above the chemical potential. The occupancy and conductance plateau might be expected to disappear once  $U_{\text{eff}}$  becomes negative around  $\lambda^2/\omega_0 \approx U/8 = 0.0625$ . Indeed, the data for  $\lambda^2/\omega_0 = 0.064$  in Fig. 9 show a narrow conductance peak that can be associated with the rapid decrease of  $\langle n_{\text{mol}} \rangle$  directly from 2 to 0 without any significant range of single occupancy [illustrated for  $\delta = 0.1$  in Fig. 10(b)].

## V. SUMMARY

We have studied the low-temperature properties of a single-molecule junction formed by a two-orbital molecule connecting metallic leads. We have investigated the low-temperature regime of the system using the numerical renormalization group to provide a nonperturbative treatment of competing strong electron-electron and electron-phonon interactions. Insight into the numerical results has been obtained by considering the phonon-renormalization of model parameters identified through canonical transformation of the starting Hamiltonian. We have focused on two quite different regions of the model's parameter space: (1) In situations where one of the two molecular orbitals lies close to the chemical potential while the other has a much higher energy, the thermodynamic properties and linear conductance are very similar to those predicted previously for a single-orbital molecule, showing phonon-induced shifts in the active molecular level and a reduction in the effective Coulomb repulsion between electrons on the molecule. (2) In the region where the two orbitals both lie close to the chemical potential, the renormalization of the Coulomb interactions is approximately four times

stronger than in the case of one active molecular level, enhancing the likelihood of attaining the interesting regime of small or even attractive on-site Coulomb interactions.

In both regions (1) and (2), electron-phonon interactions favor double occupancy of the molecule and are detrimental to formation of a molecular local moment and to the low-temperature Kondo screening of that moment by electrons in the leads. With increasing electron-phonon coupling, the Kondo effect is progressively destroyed and a phonon-dominated nonmagnetic ground state emerges in its place. In all the cases presented here, this evolution produces a smooth crossover in the ground-state properties. Special situations that result in first-order quantum phase transitions between

Kondo and non-Kondo ground states will be described in a subsequent publication.

### Acknowledgments

The authors acknowledge partial support of this work by CAPES (G.I.L), by CNPq under grant 493299/2010-3 (E.V.A.) and a CIAM grant (E.V. and E.V.A.), by FAPEMIG under grant CEX-APQ-02371-10 (E.V.A.), and by the NSF Materials World Network program under grants DMR-0710540 and DMR-1107814 (L.D. and K.I.).

- <sup>1</sup> A. Troisi and M. A. Ratner, Nano Lett. **6**, 1784 (2006).
- <sup>2</sup> A. Troisi and M. A. Ratner, Phys. Rev. B **72**, 033408 (2005).
- <sup>3</sup> W. Ho, J. Chem. Phys. **117**, 11033 (2002).
- <sup>4</sup> M. P. Trilisa, G. S. Ron, C. Marsh, and B. D. Dunietz, J. Chem. Phys. **128**, 154706 (2007).
- <sup>5</sup> Z. Liu, S.-Y. Ding, Z.-B. Chen, X. Wang, J.-H. Tian, J. R. Anema, X.-S. Zhou, D.-Y. Wu, B.-W. Mao, X. Xu, et al., Nature Communications **2**, 305 (2011).
- <sup>6</sup> M. Verdaguer, Science **272**, 698 (1996).
- <sup>7</sup> R. H. James and M. A. Ratner, Phys. Today **56**, 43 (2003).
- <sup>8</sup> R. H. M. Smith, Y. Noat, C. Untiedt, N. D. Lang, M. C. van Hemert, and J. M. van Ruitenbeek, Nature **419**, 906 (2002).
- <sup>9</sup> D. Djukic, K. S. Thygesen, C. Untiedt, R. H. M. Smit, K. W. Jacobsen, and J. M. van Ruitenbeek, Phys. Rev. B **71**, 161402 (2005).
- <sup>10</sup> K. H. Khoo, J. B. Neaton, H. J. Choi, and S. G. Louie, Phys. Rev. B **77**, 115326 (2008).
- <sup>11</sup> J. M. C. Rauba, M. Strange, and K. S. Thygesen, Phys. Rev. B **78**, 165116 (2008).
- <sup>12</sup> Z.-L. Li, B. Zou, C.-K. Wang, and Y. Luo, Phys. Rev. B **73**, 075326 (2006).
- <sup>13</sup> R. Stadler, K. S. Thygesen, and K. W. Jacobsen, Phys. Rev. B **72**, 241401 (2005).
- <sup>14</sup> S. Kubatkin, A. Danilov, M. Hjort, J. Cornil, J.-L. Brédas, N. Stühr-Hansen, P. Hedegard, and T. Bjørnholm, Nature **425**, 698 (2003).
- <sup>15</sup> J. Park, A. N. Pasupathy, J. I. Goldsmith, C. Chang, Y. Yaish, J. R. Petta, M. Rinkoski, J. P. Sethna, H. D. M. Abrua, P. L., et al., Nature **417**, 722 (2002).
- <sup>16</sup> W. Liang, M. P. Shores, M. Bockrath, J. R. Long, and H. Park, Nature **417**, 725 (2002).
- <sup>17</sup> A. C. Hewson, *The Kondo Problem to Heavy Fermions* (Cambridge University Press, 1993).
- <sup>18</sup> R. C. Jaklevic and J. Lambe, Phys. Rev. Lett. **17**, 1139 (1966).
- <sup>19</sup> J. Kirtley, D. J. Scalapino, and P. K. Hansma, Phys. Rev. B **14**, 3177 (1976).
- <sup>20</sup> B. C. Stipe, M. A. Rezaei, and W. Ho, Science **280**, 1732 (1998).
- <sup>21</sup> H. Park, J. Park, A. K. L. Lim, E. H. Anderson, A. P. Alivisatos, and P. L. McEuen, Nature (London) **407**, 57 (2000).
- <sup>22</sup> J. Gaudioso, L. J. Lauhon, and W. Ho, Phys. Rev. Lett. **85**, 1918 (2000).
- <sup>23</sup> E. M. Weig, R. H. Blick, T. Brandes, J. Kirschbaum, W. Wegscheider, M. Bichler, and J. P. Kotthaus, Phys. Rev. Lett. **92**, 046804 (2004).
- <sup>24</sup> J. G. Kushmerick, J. Lazorcik, C. H. Patterson, R. Shashidhar, D. S. Seferos, and G. C. Bazan, Nano Lett. **4**, 639 (2004).
- <sup>25</sup> K. A. Al-Hassanieh, C. A. Büsser, G. B. Martins, and E. Dagotto, Phys. Rev. Lett. **95**, 256807 (2005).
- <sup>26</sup> M. Galperin, M. A. Ratner, and A. Nitzan, J. Phys.: Condens. Matter **19**, 103201 (2007).
- <sup>27</sup> R. Härtle and M. Thoss, Phys. Rev. B **83**, 115414 (2011).
- <sup>28</sup> H. Song, Y. Kim, Y. H. Jang, H. Jeong, M. A. Reed, and L. T., Nature **462**, 1039 (2009).
- <sup>29</sup> D. Goldhaber-Gordon, H. Shtrikman, D. Mahalu, D. Abusch-Magder, U. Meirav, and M. A. Kastner, Nature **391**, 156 (1998).
- <sup>30</sup> H. Jeong, A. M. Chang, and M. R. Melloch, Science **293**, 2221 (2001).
- <sup>31</sup> E. Roca, C. Trallero-Giner, and M. Cardona, Phys. Rev. B **49**, 13704 (1994).
- <sup>32</sup> P. W. Anderson, Phys. Rev. **124**, 41 (1961).
- <sup>33</sup> T. Holstein, Ann. Phys. (N.Y.) **8**, 325 (1959).
- <sup>34</sup> E. Šimánek, Solid State Commun. **32**, 731 (1979).
- <sup>35</sup> C. S. Ting, D. N. Talwar, and K. L. Ngai, Phys. Rev. Lett. **45**, 1213 (1980).
- <sup>36</sup> H. Kaga, I. Sato, and M. Kobayashi, Prog. Theor. Phys. **64**, 1918 (1980).
- <sup>37</sup> K. Schönhammer and O. Gunnarsson, Phys. Rev. B **30**, 3141 (1984).
- <sup>38</sup> B. Alascio, C. Balseiro, G. Ortíz, M. Kiwi, and M. Lagos, Phys. Rev. B **38**, 4698 (1988);
- <sup>39</sup> H.-B. Schüttler, and A. J. Fedro, Phys. Rev. B **38**, 9063 (1988).
- <sup>40</sup> T. Östreich, Phys. Rev. B **43**, 6068 (1991).
- <sup>41</sup> A. C. Hewson and D. Meyer, J. Phys.: Condens. Matter **14**, 427 (2002).
- <sup>42</sup> G. S. Jeon, T.-H. Park, and H.-Y. Choi, Phys. Rev. B **68**, 045106 (2003).
- <sup>43</sup> J.-X. Zhu and A. V. Balatsky, Phys. Rev. B **67**, 165326 (2003).
- <sup>44</sup> H. C. Lee and H.-Y. Choi, Phys. Rev. B **69**, 075109 (2004); **70**, 085114 (2004).
- <sup>45</sup> P. S. Cornaglia, H. Ness, and D. R. Grempel, Phys. Rev. Lett. **93**, 147201 (2004).
- <sup>46</sup> P. S. Cornaglia, D. R. Grempel, and H. Ness, Phys. Rev. B **71**, 075320 (2005).
- <sup>47</sup> R. C. Monreal, F. Flores, and A. Martin-Rodero, Phys. Rev. B **82**, 235412 (2010).
- <sup>48</sup> J. Hubbard, Proc. Roy. Soc. (London) **A276**, 238 (1963).
- <sup>49</sup> E. Vernek, E. V. Anda, S. E. Ulloa, and N. Sandler, Phys. Rev. B **76**, 075320 (2007).
- <sup>50</sup> A. Goker, J. Phys.: Condens. Matter **23**, 125302 (2011).
- <sup>51</sup> K. G. Wilson, Rev. Mod. Phys. **47**, 773 (1975).



- <sup>52</sup> H. R. Krishna-murthy, J. W. Wilkins, and K. G. Wilson, Phys. Rev. B **21**, 1003 (1980); **21**, 1044 (1980).
- <sup>53</sup> R. Bulla, T. A. Costi, and T. Pruschke, Rev. Mod. Phys. **80**, 395 (2008).
- <sup>54</sup> W. Hofstetter and H. Schoeller, Phys. Rev. Lett. **88**, 016803 (2002).
- <sup>55</sup> A. Kogan, G. Granger, M. A. Kastner and D. Goldhaber-Gordon, Phys. Rev. B **67**, 113309 (2003).
- <sup>56</sup> N. Roch, S. Florens, V. Bouchiat, W. Wernsdorfer and F. Balestro, Nature **453**, 633 (2008).
- <sup>57</sup> I. G. Lang and Y. A. Firsov, Zh. Eksp. Teor. Fiz. **43**, 1843 (1962).
- <sup>58</sup> P. L. Fernas, F. Flores, and E. V. Anda, J. Phys. Condens. Matter **4**, 5309 (1992).
- <sup>59</sup> D. E. Logan, C. J. Wright, and M. R. Galpin, Phys. Rev. B **80**, 125117 (2009).